The Journal of Neuroscience, October 1, 2002, 22(19):8487–8503

Distal Extension of Climbing Fiber Territory and Multiple Innervation Caused by Aberrant Wiring to Adjacent Spiny Branchlets in Cerebellar Purkinje Cells Lacking Glutamate Receptor δ2

Ryoichi Ichikawa,[1,2] Taisuke Miyazaki,[1] Masanobu Kano,[3] Tsutomu Hashikawa,[4] Haruyuki Tatsumi,[2] Kenji Sakimura,[5] Masayoshi Mishina,[6] Yoshiro Inoue,[1] and Masahiko Watanabe[1]

[1]Department of Anatomy, Hokkaido University School of Medicine, Sapporo 060-8638, Japan, [2]Department of Anatomy, Sapporo Medical University School of Medicine, Sapporo 060-8556, Japan, [3]Department of Physiology, Kanazawa University School of Medicine, Takara-machi, Kanazawa 920-8640, Japan, [4]Laboratory for Neural Architecture, Brain Science Institute, RIKEN, Wako 351-0198, Japan, [5]Department of Cellular Neurobiology, Brain Research Institute, Niigata University, Niigata 951-8122, Japan, and [6]Department of Molecular Neurobiology and Pharmacology, Graduate School of Medicine, University of Tokyo, and Solution-Oriented Research for Science and Technology, Japan Science and Technology, Tokyo 113-0033, Japan

Organized synapse formation on to Purkinje cell (PC) dendrites by parallel fibers (PFs) and climbing fibers (CFs) is crucial for cerebellar function. In PCs lacking glutamate receptor δ2 (GluRδ2), PF synapses are reduced in number, numerous free spines emerge, and multiple CF innervation persists to adulthood. In the present study, we conducted anterograde and immunohistochemical labelings to investigate how CFs innervate PC dendrites under weakened synaptogenesis by PFs. In the GluRδ2 knock-out mouse, CFs were distributed in the molecular layer more closely to the pial surface compared with the wild-type mouse. Serial electron microscopy demonstrated that CFs in the knock-out mouse innervated all spines protruding from proximal dendrites of PCs, as did those in the wild-type mouse. In the knock-out mouse, however, CF innervation extended distally to spiny branchlets, where nearly half of the spines were free of innervation in contrast to complete synapse formation by PFs in the wild-type mouse. Furthermore, from the end point of innervation, CFs aberrantly jumped to form ectopic synapses on adjacent spiny branchlets, whose proximal portions were often innervated by different CFs. Without GluRδ2, CFs are thus able to expand their territory along and beyond dendritic trees of the target PC, resulting in persistent surplus CFs by innervating the distal dendritic segment. We conclude that GluRδ2 is essential to restrict CF innervation to the proximal dendritic segment, by which territorized innervation by PFs and CFs is properly structured and the formation of excess CF wiring to adjacent PCs is suppressed.

Key words: cerebellum; Purkinje cell; climbing fiber; multiple innervation; parallel fiber; glutamate receptor δ2

The cerebellum receives two excitatory afferents, the climbing fiber (CF) and mossy fiber (Palay and Chan-Palay, 1974). CFs originating in the inferior olive innervate the proximal dendritic segment of Purkinje cells (PCs). Mossy fibers convey massive signals to the distal dendritic segment called spiny branchlets via parallel fibers (PFs), granule cell axons. When coactivated with CF input, PF synapses undergo long-term depression (LTD), a form of synaptic plasticity thought to underlie cerebellar motor learning (Ito, 1989; Linden and Connor, 1995). Adult PCs are innervated by single CFs, but this one-to-one relationship is preceded by a transitory stage of multiple innervation (Mariani and Changeux, 1981a,b; Crépel, 1982). Analyses of "agranular" and "hypogranular" cerebella, in which PF→PC synapses are severely depleted by genetic mutation or antimitotic treatment, have demonstrated that PF→PC synaptogenesis is a prerequisite for developmental elimination of surplus CFs (Woodward et al., 1974; Crépel, 1982; Mariani, 1982). Gene knock-out studies have uncovered that intact glutamatergic signaling at PC synapses is important for synapse development, LTD induction, and motor learning (Aiba et al., 1994; Conquet et al., 1994; Kano et al., 1995, 1997, 1998; Kashiwabuchi et al., 1995; Offermanns et al., 1997; Ichise et al., 2000).

Glutamate receptor δ2 (GluRδ2) is expressed exclusively in PCs (Araki et al., 1993; Lomeli et al., 1993), and localized selectively at PF→PC synapses in the adult brain (Landsend et al., 1997). Although ligands and properties of GluRδ2 receptors are still unclear, the lurcher mutation of the GluRδ2 gene in mice yields constitutively active channels causing spontaneous PC degeneration and ataxia (Zuo et al., 1997; Kohda et al., 2000; Wollmuth et al., 2000). In the GluRδ2 knock-out mouse, cerebellar histoarchitecture is grossly normal, and PCs develop arborized dendrites studded with numerous spines (Kashiwabuchi et al., 1995). However, the knock-out mouse is impaired in PF synaptogenesis, elimination of surplus CFs, LTD induction, motor coordination, and motor learning (Funabiki et al., 1995; Kashiwabuchi et al., 1995; Kishimoto et al., 2001). The lowering

Received Nov. 14, 2001; revised June 5, 2002; accepted June 10, 2002.

This work was performed through special coordination funds for promoting science and technology and through a grant-in-aid for Scientific Research (A), both provided by the Ministry of Education, Culture, Sports, Science and Technology of the Japanese Government and was also supported in part by the Novartis Foundation (Japan) for the Promotion of Science and by Takeda Science Foundation.

Correspondence should be addressed to Masahiko Watanabe, Department of Anatomy, Hokkaido University School of Medicine, Sapporo 060-8638, Japan. E-mail: watamasa@med.hokudai.ac.jp.

of the synaptic contact rate of PC spines with PF terminals leads to a reduced PF synapse number to half the level of wild-type PCs, and numerous free spines emerge, indicating the role in selective strengthening of PF→PC synapses (Kurihara et al., 1997). In the null-type GluRδ2 mutation hotfoot, the generation of free spines has also been reported (Guastavino et al., 1990; Lalouette et al., 2001).

In the present study, we used CF labeling and serial electron microscopy to investigate how the incomplete PF synaptogenesis affects CF innervation using the knock-out mouse. Here we show that CF innervation extends distally to spiny branchlets and further jumps to form ectopic synapses on adjacent branchlets, resulting in multiple innervation by different CFs. Therefore, GluRδ2 is essential to restrict CF innervation to the proximal dendritic segment of the target PC. Together with the fact that PFs invade the proximal dendritic segment when CFs are deleted or inactivated (Strata and Rossi, 1998), the two inputs are highly competitive and plastic, each being able to expand its own territory at the expense of the other.

MATERIALS AND METHODS

Animals. The GluRδ2 knock-out mouse was produced by homologous recombination as described previously (Kashiwabuchi et al., 1995). Heterozygous pairs on a C57BL/6 × CBA genetic background were mated to obtain the knock-out and wild-type offspring. The genotype was determined by PCR using a mixture of allele-specific forward primers and a common reverse primer, as reported previously (Takeuchi et al., 2001).

Anterograde labeling. Under deep anesthesia with chloral hydrate (350 mg/kg of body weight, i.p.), a glass pipette (inner tip diameter, 10–20 μm) filled with 2–3 μl of 10% solution of biotinylated dextran amine (molecular weight, 10,000; Molecular Probes, Eugene, OR) in PBS, was inserted to the right medial accessory olivary nucleus by the dorsal approach (Rossi et al., 1995). Biotinylated dextran amine was injected iontophoretically by a 7 μA positive current for 30 min with a protocol of 700 msec on and 1300 msec off. After 6–8 d of survival, mice were anesthetized with chloral hydrate (350 mg/kg) and perfused transcardially with 4% paraformaldehyde in 0.1 M phosphate buffer (PB), pH 7.4, for light microscopy or with 0.1% glutaraldehyde and 4% paraformaldehyde in 0.1 M PB for electron microscopy. Brains were excised quickly from the skull and immersed overnight in the same fixative, followed by a rinse in 0.1 M PB for at least 1 d.

Light microscopy. For visualization of labeled CFs, microslicer sections through the cerebellar vermis (50 μm in thickness, DKT-1500; Dosaka, Kyoto, Japan) were prepared in the parasagittal plane. Sections were incubated overnight in streptavidin-horseradish peroxidase (Amersham Biosciences, Buckinghamshire, UK) diluted with 0.1 M PB containing 1% Tween 20 and visualized with diaminobenzidine (DAB) and cobalt. Low-power photographs were taken with a Normarski interference contrast microscope (Axiophoto; Zeiss, Gutingen, Germany), whereas high-power photographs were taken with a bright-field microscope (AX-80; Olympus Optical, Tokyo, Japan). To evaluate quantitative differences in the extent of labeled CFs and the number of terminal tendrils, 10 CFs were analyzed in each of the three knock-out and three wild-type mice. The p value was calculated using Student's t test.

Immunofluorescence. To visualize CF terminals by immunohistochemistry, we produced guinea pig antibody against vesicular glutamate transporter DNPI (or VGLUT2). Antigen (amino acid residues 519–582 of the rat DNPI; GenBank accession number AAF76223) was obtained by bacterial expression as a glutathione *S*-transferase fusion protein using pGEX4T-1 plasmid (Amersham Biosciences, Uppsala, Sweden). The fusion protein was purified using glutathione-Sepharose (Amersham Biosciences), emulsified with Freund's complete adjuvant (Difco, Detroit, MI), and injected subcutaneously into female a Hartley guinea pig at intervals of 2 weeks. From the antiserum sampled 2 weeks after the sixth injection, affinity-purified antibodies were prepared, first using protein G-Sepharose (Amersham Biosciences) and then using antigen peptides coupled to CNBr-activated Sepharose 4B (Amersham Biosciences). For the preparation of affinity media, DNPI polypeptide was obtained by elution of cleaved polypeptide after in-column thrombin digestion of fusion proteins bound to glutathione-Sepharose.

For double immunofluorescence, microslicer sections were incubated overnight with a mixture of guinea pig DNPI antibody (0.5 μg/ml) and rabbit calbindin antiserum (1:10,000; Nakagawa et al., 1998) and visualized by a 1 hr incubation with Cy3- or FITC-labeled species-specific secondary antibodies (1:200; Jackson ImmunoResearch, West Grove, PA). For DNPI immunofluorescence combined with anterograde CF labeling, biotinylated dextran amine was first visualized by a 1 hr incubation with 2 μg/ml streptavidin-Alexa 594 (Molecular Probes) and then by overnight incubation with guinea pig DNPI antibody (0.5 μg/ml) followed by Cy3-labeled anti-guinea pig IgG. Images were scanned using a confocal laser microscope (Fluoview; Olympus), and five images acquired at different levels along the z-axis were compiled into single images.

Electron microscopy. For electron microscopy, parasagittal microslicer sections (50 μm) through the cerebellar vermis were incubated overnight in streptavidin-horseradish peroxidase diluted with 0.1 M PB containing 0.5% Tween 20 and visualized with DAB. Sections were postfixed for 30 min with 1% osmium tetroxide in 0.1 M PB, block-stained overnight with 1% aqueous uranyl acetate solution, dehydrated using graded alcohols, and embedded in Epon 812. To reconstruct the labeled CFs innervating PC dendrites, sets of 1500–1800 ultrathin sections were prepared serially by cutting Epon blocks in the plane parallel to the pial surface. Sections were made using an Ultracut E ultramicrotome (Reichert-Jung, Vienna, Austria) by setting the section thickness at 100 nm. A ribbon of serial sections, each consisting of at least 20 sections, was mounted on a single-slot copper grid (1 × 2 mm) supported with a Formvar membrane. Electron micrographs were taken from every second section with an H7100 electron microscope (Hitachi, Tokyo, Japan) at an original magnification of 5000× and printed at the final magnification of 10,000×. Three-dimensional images of dendritic spines were reconstructed by stacking their outlines from micrographs and smoothing with a black–white gradient painting.

Combined anterograde and immunohistochemical labelings for CFs were also used. Parasagittal cerebellar sections were first subjected to pre-embedding silver-enhanced immunogold for the visualization of DNPI-immunolabeled CF terminals. In immunogold labeling, sections were immunoreacted with guinea pig DNPI antibody (2 μg/ml) overnight and with anti-guinea pig IgG covalently linked to 1.4 nm gold particles (Nonogold; Nanoprobes, Stony Brook, NY) for 6 hr. After silver enhancement (HQ silver; Nanoprobes), sections were then incubated overnight with streptavidin-horseradish peroxidase for the visualization of anterogradely labeled CFs. Double-labeled sections were osmificated and embedded in Epon as above for serial electron microscopy.

RESULTS

The right medial accessory olivary nucleus of the GluRδ2$^{-/-}$ (knock-out) and GluRδ2$^{+/+}$ (wild-type) mice at 2–4 months of age was iontophoretically injected with biotinylated dextran amine. After 6–8 d of survival, the site and extent of injection were examined in coronal brainstem sections (Fig. 1*A,B*). Brains with restricted intranuclear injection were selected for visualization of anterogradely labeled CFs in the cerebellum. We analyzed labeled CFs, whose trajectories can be thoroughly traced in single sections at the straight portion of lobules 4/5 and 6. In each analysis, we collected data using three wild-type and three knock-out mice.

Light microscopic analysis

In the wild-type and GluRδ2 knock-out mice, labeled axons running through the granular and PC layers were thin, smooth fibers (Fig. 2*A,B*, *arrows*). When reaching the base of the molecular layer, they thickened and started branching in the parasagittal plane (Figs. 1*C,D*, 2*C,D*). While ascending the molecular layer, these branches gave off beaded tendrils into various directions. Fluorescent double staining showed that varicosities of labeled fibers (Fig. 1*C,D*, *red*) contained DNPI-like immunoreactivity (*green*), thus yielding yellowish puncta along the entire course of labeled fibers. Because DNPI is a vesicular glutamate transporter specific to CF terminals in the molecular layer of the adult cerebellum (Fremeau et al., 2001), all of these features indicate successful anterograde labeling of CFs. Even at the light micro-

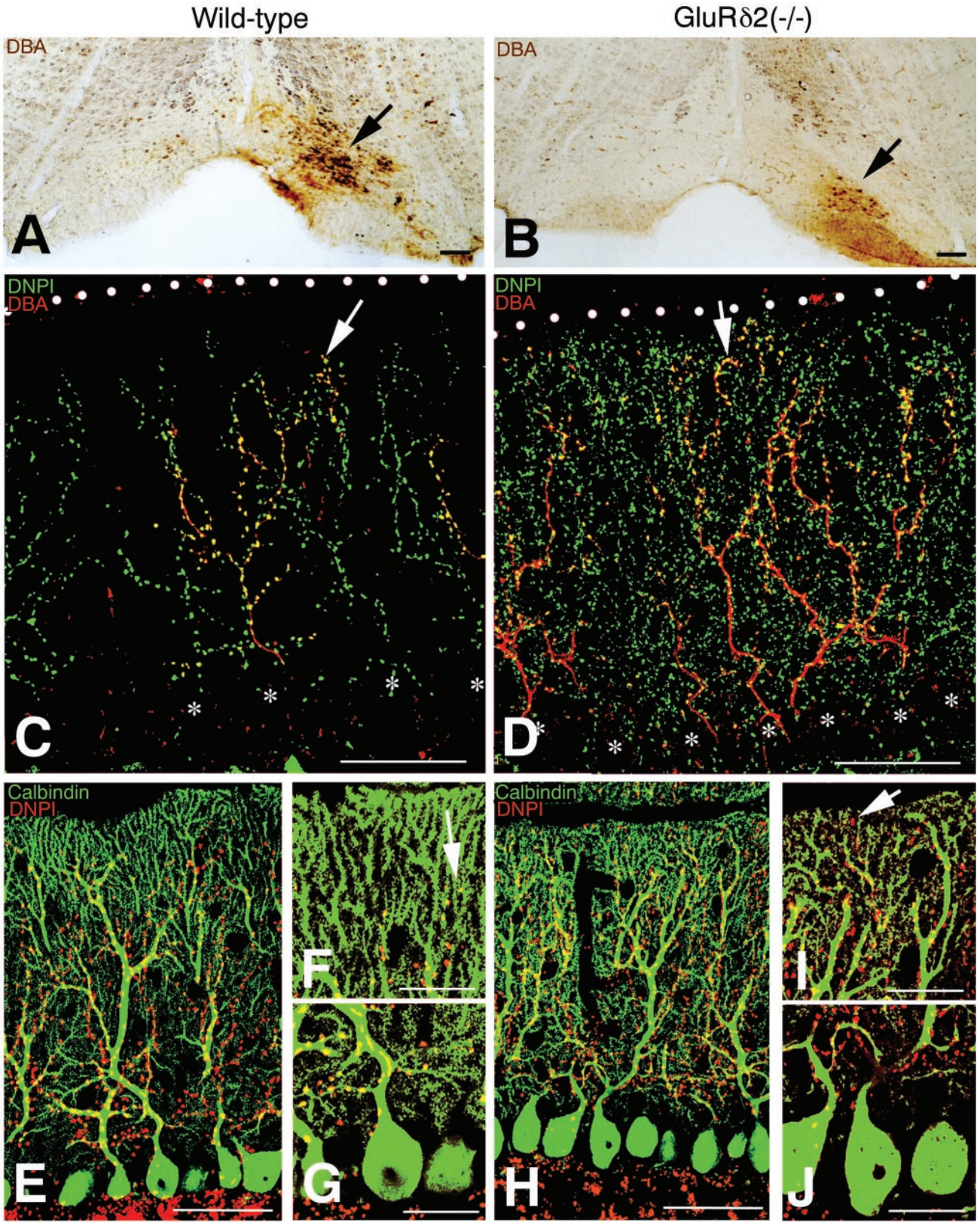

Figure 1. CF labeling in the wild-type (*A, C, E–G*) and GluRδ2 knock-out (*B, D, H–J*) mice. *A, B*, Injection site and extent (*arrows*) of biotinylated dextran amine (BDA) in the inferior olivary nucleus. *C, D*, Double fluorescence for BDA-labeled CFs (*red*) and vesicular glutamate transporter DNPI (*green*). *Arrows* indicate the tips of BDA-labeled CFs. *White dots* and *asterisks* indicate the pial surface of the cerebellum or PC somata, respectively. Note an expanded distribution of both BDA- and DNPI-labeled CFs in the knock-out molecular layer. Also note a marked increase of DNPI-immunolabeled puncta in the knock-out molecular layer. *E–J*, Double immunofluorescence for DNPI (*red*) and calbindin (*green*). *F, I*, and *G, J*, Closer views of the superficial and deep portions of the molecular layer shown in *E* and *H*, respectively. *Arrows* indicate the most superficial puncta immunostained for DNPI. Scale bars: *A, B*, 100 μm; *C–E, H*, 50 μm; *F, G, I, J*, 20 μm.

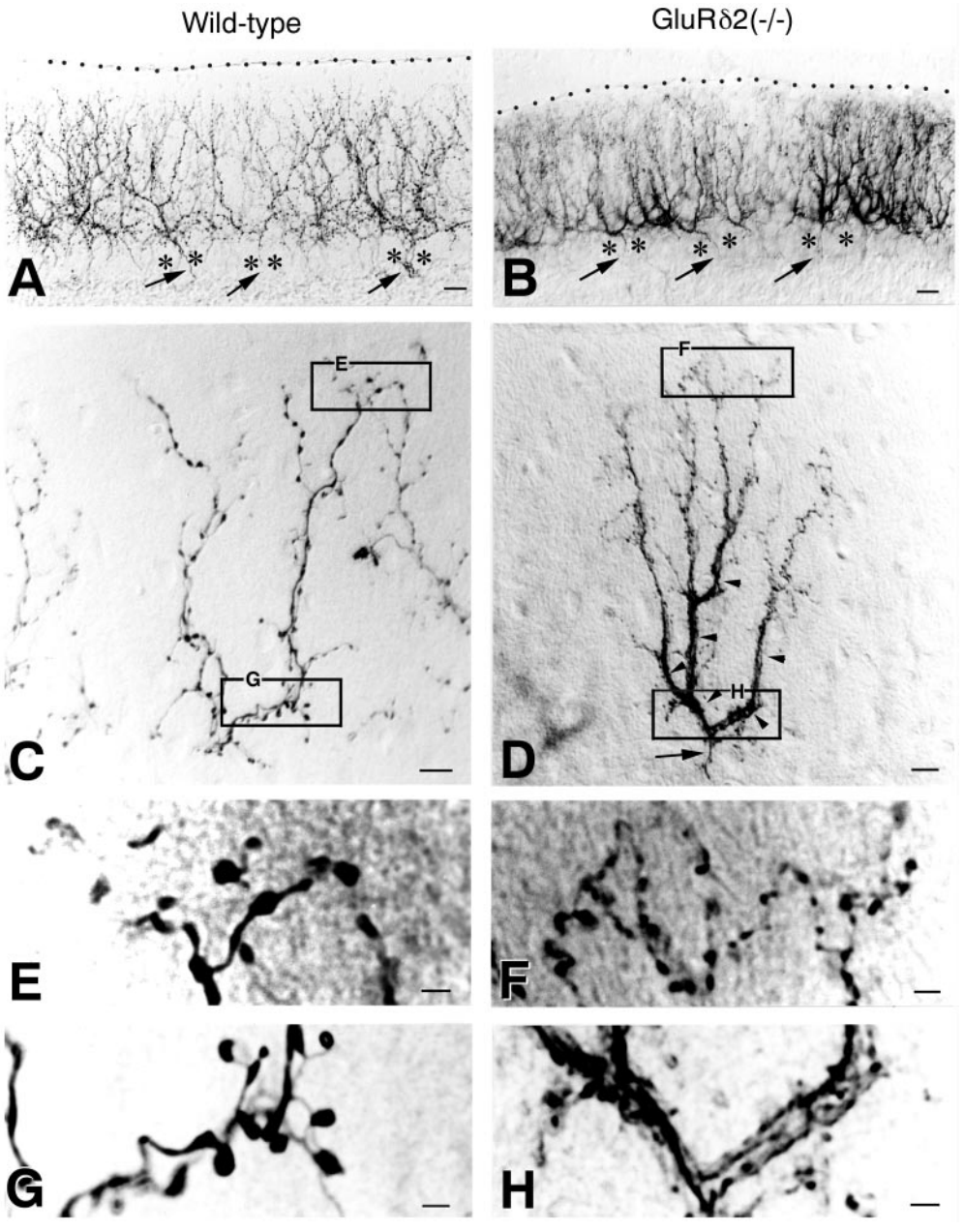

Figure 2. Anterogradely labeled CFs in lobule VI of the wild-type (*A, C, E, G*) and GluRδ2 knock-out (*B, D, F, H*) cerebella. *A, B*, Low-power views of cerebellar regions with massive CF labeling. The pial surface is indicated by the *dotted line*. *Arrows* indicate thin labeled axons, which run through the granular layer and between PC somata (*asterisk*). *C, D*, CFs with isolated labeling. *Arrowheads* in *D* indicate the dense, plexus-like innervation characteristic of the knock-out mouse. *E, F*, High-power views of the *top portions* in *C* and *D*. CF tendrils having small terminal boutons are increased in the knock-out mouse. *G, H*, High-power views of the *bottom portions* in *C* and *D*. A dense, plexus-like innervation is conspicuous in the knock-out mouse. Scale bars: *A, B*, 20 μm; *C, D*, 10 μm; *E–H*, 2 μm.

scopic level, phenotypic differences were clearly noted in the distribution and morphology of labeled CFs.

First, labeled CFs in the knock-out mouse were distributed more closely to the pial surface than those in the wild-type mouse (Figs. 1*C,D*, 2*A,B*). Because the thickness of the molecular layer is slightly reduced in the GluRδ2 knock-out mouse (Kurihara et al., 1997), we evaluated the difference by measuring the vertical height to the most distal tip of anterogradely labeled CFs relative to the molecular layer thickness. We measured 10 labeled CFs from each mouse, and the scores were averaged to represent that particular mouse. The mean relative height of labeled CFs was 83.9 ± 0.5% and 95.1 ± 0.4% of the molecular layer thickness in the wild-type and knock-out mice, respectively, showing a significant difference (mean ± SE; *t* test; $p < 0.0001$). The difference was further confirmed by double immunofluorescence for DNPI and calbindin (Fig. 1*E–J*). In the wild-type mouse, most DNPI-immunopositive puncta were associated with primary and secondary dendrites having smooth contours (Fig. 1*E,G*). Only a few puncta were observed around proximal portions of spiny branchlets, leaving a DNPI immunofluorescence-free zone in the superficial one-fifth or one-sixth of the molecular layer (Fig. 1*F*). In the knock-out mouse, DNPI-immunopositive puncta were found around many portions of spiny branchlets, and again they were distributed close to the pial surface (Fig. 1*H–J*).

Second, the formation of plexus-like CF bundles was conspicuous in the lower half of the knock-out molecular layer (Fig. 2*C,D,G,H*). The plexus consisted of multiple branches and tendrils, appeared abruptly at the base of the molecular layer, and stemmed from a single thin fiber running up the granular layer (Fig. 2*B,D*). Third, terminal tendrils, which were fine-beaded collaterals emitting from thick stem branches of CFs, were more numerous in the knock-out mouse (Fig. 2*C,D*). We compared the difference by counting the number of terminal tendrils in the upper half of the molecular layer, because the plexus formation

hindered the identification of individual tendrils in the lower molecular layer. The mean number of terminal tendrils in the upper half of the molecular layer, obtained by measuring 10 labeled CFs from each mouse, was 24.7 ± 0.8 in the wild-type and 53.4 ± 1.1 in the knock-out mouse, showing a significant difference ($p < 0.0001$). Fourth, boutons on CF tendrils were smaller and more numerous in the knock-out mouse than in the wild-type mouse (Fig. 2*E,F*). Reflecting these changes, a substantial increase of DNPI-immunopositive puncta was noted in the molecular layer of the knock-out mouse (Fig. 1*D, green puncta*, *H–J, red puncta*).

Electron microscopic analysis

For electron microscopic analysis, we selected from CF branches a particular track that ran straight and vertically to the pial surface. Along the selected track, innervation patterns were examined from the base to the distal end of PC dendrites by preparing serial ultrathin sections in the horizontal plane (i.e., the plane parallel to the pia mater) (Figs. 3–8) and were reconstructed schematically (Fig. 9). Labeled CFs were readily identified by the presence of electron-dense labeled substance. We also identified unlabeled CFs and distinguished them from PFs by their different morphology and trajectory. Unlabeled CFs formed large terminal boutons having densely packed synaptic vesicles and relatively dark cytoplasm. Moreover, each terminal bouton of CFs made synaptic contact with two or more spines protruding from the associating dendrites, as described previously (Palay and Chan-Palay, 1974; Xu-Friedman et al., 2001). On the other hand, PFs were bundled axons running transversely in such horizontal sections; they formed small boutons containing relatively few synaptic vesicles and made synaptic contact with single or at most two spines protruding from small-caliber spiny dendrites. For descriptive convenience, we categorized dendritic trees of PCs into three domains, as originally noted by Larramendi and Victor (1967): the PC domain I (PCD-I) innervated by CFs but not by PFs (Fig. 9, *dark blue*), PCD-II with mixed CF–PF innervation (*light blue*), and PCD-III innervated by PFs but not by CFs (*green*). In the two strains of mice, ordered arrangement from PCD-I to PCD-III was preserved along the proximal-to-distal axis of dendritic trees (Fig. 9). The spine density at each dendritic domain did not differ significantly between the two types of mice (Figs. 3*A*, 4*A*, 5*A*). However, phenotypic differences were observed in the pattern of innervation and the vertical length of respective dendritic domains (Figs. 3–5, Table 1).

PCD-I or proximal domain (Fig. 3)

In both types of mice, the PCD-I domain had large-caliber dendrites with morphological characteristics of low spine density (Fig. 3*A*), a high content of microtubules, and low occupancy by mitochondria (Fig. 3*C,F*). In the domain, all spines were innervated by labeled CFs only (Fig. 3*B*), and innervation by unlabeled CFs was not observed in any of three cases examined for the wild-type or knock-out mouse (Fig. 9). The most notable difference in the PCD-I domain was a dense association of CFs in the knock-out mouse (Fig. 3*C,E,F,H*). When counting CF profiles at 10 μm above the initial branching point of CFs, the profile number per dendrite was 2, 3, and 5 in three wild-type mice and 15, 17, and 24 in three knock-out mice, showing a marked difference. In both mice, all of these CF branches were confirmed to arise from a single parent fiber, i.e., collaterals (Fig. 9). Between the two types of mice, branching patterns of CFs were different; branching was almost dichotomous in the wild-type mouse (Figs. 3*D,E*, 9), whereas in the knock-out mouse, individual CFs produced as many as four to seven branches, especially at the proximal portion of the PCD-I domain (Figs. 3*G,H*, 9). The size of terminal boutons was compared by measuring the short diameter of the largest terminal profiles for 12 boutons in each mouse. Consistent with light microscopic observation, the mean short diameter was significantly decreased in the knock-out mouse (0.85 ± 0.01 μm in wild type and 0.74 ± 0.01 μm in knock-out; $p < 0.02$).

The vertical length of dendrites was estimated from the number and thickness (100 nm) of serial ultrathin sections (Table 1). In accordance with a slight reduction of the molecular layer thickness, the total vertical length of measured dendrites was slightly diminished in knock-out mice (knock-out/wild-type ratio, 0.91; Table 1). When the length of each dendritic domain was compared as the proportional length relative to the total dendritic length, the proportional length of the PCD-I domain was moderately but significantly reduced in the knock-out mouse (knock-out/wild-type ratio, 0.76; $p < 0.01$; Table 1).

PCD-II or intermediate domain (Fig. 4)

In both mice, the PCD-II domain was characterized by high spine density (Fig. 4*A*) and mixed CF–PF innervation (Fig. 4*B*). In the domain, several phenotypic differences were clear. First, all PC spines were contacted by either CFs or PFs in the wild-type mouse, whereas free spines emerged in the knock-out mouse (free spines, 0% in the wild type and 37.4 ± 2.2% in the knock-out) (Fig. 4*B*). Figure 4, *C* and *E1*, shows a typical case in the wild-type mouse; of the three marked spines protruding from the PCD-II domain, spine S3 was innervated by labeled CF and spines S1 and S2 were contacted by PFs running transversely (longitudinally in these photographs). Figure 4, *D* and *F1*, shows a case in the knock-out mouse; spines S1 and S4 were contacted by labeled CF or PF, respectively, whereas spines S2 and S3 on the same dendrite were free of innervation. In such free spines, postsynaptic density-like condensation (Fig. 4*D1,D3*, *arrowheads*) was present, but it was much smaller (Fig. 4*F2*) than that in the contacted spines of wild-type and knock-out mice (Fig. 4*E2*). Free spines were thoroughly surrounded by cytoplasmic sheets of Bergmann glia.

Second, the fraction of PC spines contacted by PFs was significantly reduced in the knock-out mouse (68.4 ± 5.2% in the wild type and 26.1 ± 1.8% in the knock-out; $p < 0.005$), whereas that of CF synapses was not altered significantly (31.6 ± 5.1% for wild type and 36.5 ± 0.9% for knock-out; $p > 0.2$) (Fig. 4*B*). Third, the vertical length of the PCD-II domain was greatly elongated in the knock-out mouse (Fig. 9). The knock-out/wild-type ratio of the proportional length was 2.48 in the PCD-II domain ($p < 0.001$; Table 1). Fourth, the distal portion of the knock-out PCD-II domain was very similar in morphology to spiny branchlets (Fig. 4*D*), i.e., small-caliber dendrites (<2 μm in diameter) with sparse microtubules and abundant mitochondria (Palay and Chan-Palay, 1974). Fifth, similarly to the PCD-I domain, the size of CF boutons was smaller in the knock-out mouse (0.65 ± 0.03 μm) than in the wild-type mouse (0.73 ± 0.02 μm; $p < 0.001$).

PCD-III or distal domain (Fig. 5)

In both mice, the PCD-III domain consisted of typical spiny branchlets, which had the highest spine density among the three domains (Fig. 5*A*) and lacked CF innervation (Fig. 5*B*). Spines in the PCD-III domain were all innervated by PFs in the wild-type

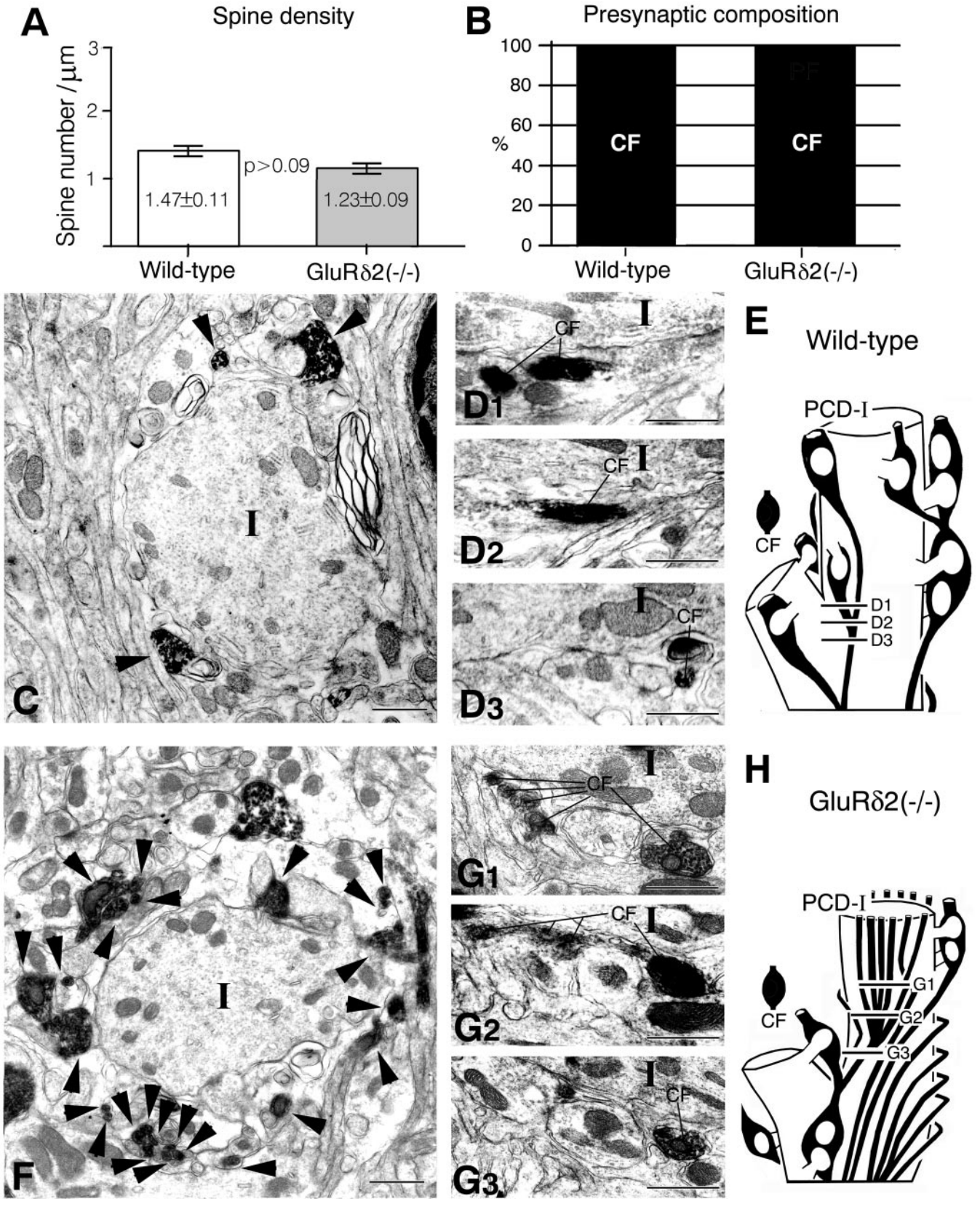

Figure 3. PCD-I (proximal) domain. *A*, Spine density. *Vertical bars* indicate the mean spine number/1 μm of dendritic length (mean ± SEM). The spine density is obtained from serial electron micrographs. *B*, Presynaptic composition on PC spines. *C–E*, Wild type. *F–H*, Knock-out. *C, F*, Cross-section images at 10 μm above the initial branching point of CFs. In *C* and *F*, note a marked increase of CF profiles (*arrowheads*) around PCD-I dendrite (*I*) in the knock-out. Single CFs usually divide into two branches in the wild-type (*D1–D3*), whereas four or more branches are produced in the knock-out (*G1–G3*). *E, H*, Reconstructed images of a part of the PCD-I domain. Approximate positions of electron micrographs *D1–D3* and *G1–G3* are indicated in the reconstructed images. Scale bars, 1 μm.

Table 1. Vertical length of the PCD-I, -II, and -III domains and their proportional length relative to the total dendritic length

	GluRδ2 knock-out	Wild type	Ratio	*p*
Vertical length (μm)[a]				
PCD-I	61.0 ± 0.5	88.9 ± 5.1	0.76	0.016
PCD-II	54.2 ± 3.3	23.4 ± 1.9	2.24	0.002
PCD-III	5.2 ± 0.5	18.0 ± 1.0	0.29	0.001
Total	117.9 ± 3.6	130.2 ± 6.7	0.91	0.10
Proportion (%)[b]				
PCD-I	51.8 ± 1.9	68.2 ± 0.9	0.76	0.003
PCD-II	44.3 ± 1.5	17.9 ± 0.6	2.48	0.001
PCD-III	3.8 ± 0.4	13.9 ± 1.2	0.27	0.005
Total (%)	100	100		

[a]The vertical length of each dendritic domain was obtained by section number and thickness (100 nm); mean ± SEM; $n = 3$.
[b]The proportion of each dendritic domain was obtained as the percentage in a given dendrite; mean ± SEM; $n = 3$.

mouse (Fig. 5*B–D*). In the knock-out mouse, 43.9 ± 0.8% of spines were contacted by PFs, whereas 55.7 ± 1.7% were free spines (Fig. 5*B,E,F*). A marked reduction in the vertical length of the PCD-III domain was found for the knock-out mouse; the knock-out/wild-type ratio of the proportional length was 0.27 in the PCD-III domain ($p < 0.005$; Table 1).

As reported in hotfoot mutant mice (Lalouette et al., 2001), a mismatch in lengths of presynaptic and postsynaptic differentiations was observed in a few PF→PC and CF→PC synapses at each PCD domain. The length of the postsynaptic specialization exceeds that of the synaptic junction between PF and spine S2 (Fig. 5*E1*, *arrow*) and between labeled CF and spine S1 (Fig. 7*I2*, *arrow*).

Aberrant innervation against adjacent spiny branchlets (Figs. 6–8)

In the wild-type mouse, innervation by each CF branch was confined to its associating track of dendrites. In contrast, CFs in the knock-out mouse frequently innervated spines on neighboring dendrites (Figs. 6, 7). Always, the target of aberrant innervation was spiny branchlets in the neighbor, which were innervated by PFs except the aberrant CF. Thus we classified the aberrantly innervated spiny branchlets as the PCD-III domain.

In Figure 6, a labeled CF innervating the PCD-II domain abruptly formed a synaptic contact with spine S2 (Fig. 6*B,C*), which protruded from the adjacent PCD-III dendrite (Fig. 6*D*). In this case, the latter dendrite was a branch of the former (Fig. 6*F,G*). Therefore, this represents aberrant CF innervation within dendritic trees of the same PC. This type of aberrant innervation (i.e., intradendritic type) occurred from any portions of CFs along their course (Fig. 9).

Another case is shown in Figure 7. A labeled CF ascended the PCD-II dendrite D1 and formed a synapse with spine S1 (Fig. 7*E,I*). It jumped to innervate successively three adjacent PCD-III dendrites: D2 (Fig. 7*B,J*, spine *S2*), D3 (Fig. 7*C,D,K*, spines *S3, S4*), and D4 (Fig. 7*D*, spine *S5*). In this case, we tried to trace back their origin but were not able to address whether D1–D4 dendrites originated from the same PC. Instead, we found unlabeled CFs (uCF1 and uCF2), both of which had large terminals with densely packed synaptic vesicles, and innervated proximal portions of the D2 (Fig. 7*F–H,L*, spine *S6*) and D3 dendrites (Fig. 7*F–H,M*, spines *S7, S8*), respectively. This type of aberrant innervation thus resulted in a dual innervation by different CFs (i.e., multiple type). We confirmed this by combined anterograde labeling and DNPI immunolabeling (Fig. 8). When spiny branchlets innervated by anterogradely labeled CFs (Fig. 8*A,B,F1,F2*, spines *S1, S2*) were traced back by serial electron microscopy, proximal portions of the dendrite were innervated by CFs that were unlabeled anterogradely but labeled for DNPI (Fig. 8*E,G*, *uCF*). Figure 8*H* is a reconstructed image of a set of serial sections shown in Figure 8*A–G*, and Figure 8*I* is another case obtained from a different set of serial sections. The multiple type of aberrant CF innervation occurred preferentially from the distal end point of innervation on to the main target PC (Fig. 9, *red asterisks*) and was encountered in all three cases analyzed in the knock-out mouse but none of the three cases in the wild-type mouse.

DISCUSSION

We investigated CF innervation in the GluRδ2 knock-out cerebellum and have disclosed its unique features, as schematically summarized in Figure 10.

Distal extension of CF territory

CFs in the GluRδ2 knock-out mouse were extended close to the pial surface of the molecular layer and produced many tendrils bearing numerous tiny boutons. In the knock-out mouse, dendritic spines on the PCD-I domain were all recruited to form CF synapses, similarly to the wild-type mouse. The PCD-II domain was markedly elongated, maintaining the fraction of PC spines contacted by CFs. Furthermore, CF innervation was further extended to spiny branchlets, where the spines in wild-type animals are contacted exclusively by PFs (Palay and Chan-Palay, 1974; Napper and Harvey, 1988). In contrast, the fraction of PC spines contacted by PFs was significantly reduced in the PCD-II domain (Fig. 4*B*), and the reduction continued to the PCD-III domain (Fig. 5*B*). Therefore, dendritic trees of GluRδ2-deficient PCs are characterized by distal extension of CF innervation under incomplete PF synaptogenesis. This pattern of innervation is different from that occurring after surgical lesions to PFs in the adult rat cerebellum, where remaining PFs immediately sprout, take over spines from degenerating PFs, and regenerate PF synapses (Chen and Hillman, 1982).

The growth of PC dendrites is slow during the first 10 d of rodents' lives and accelerates in the next 10 d (Altman, 1972). Simultaneously with dendritic differentiation, the bulk of granule cells come into existence and project PFs in the superficial molecular layer, where they interact with growing PC dendrites to form immature synapses (Woodward et al., 1971; Altman, 1972; Takács and Hámori, 1994). Concomitant with PF synaptogenesis,

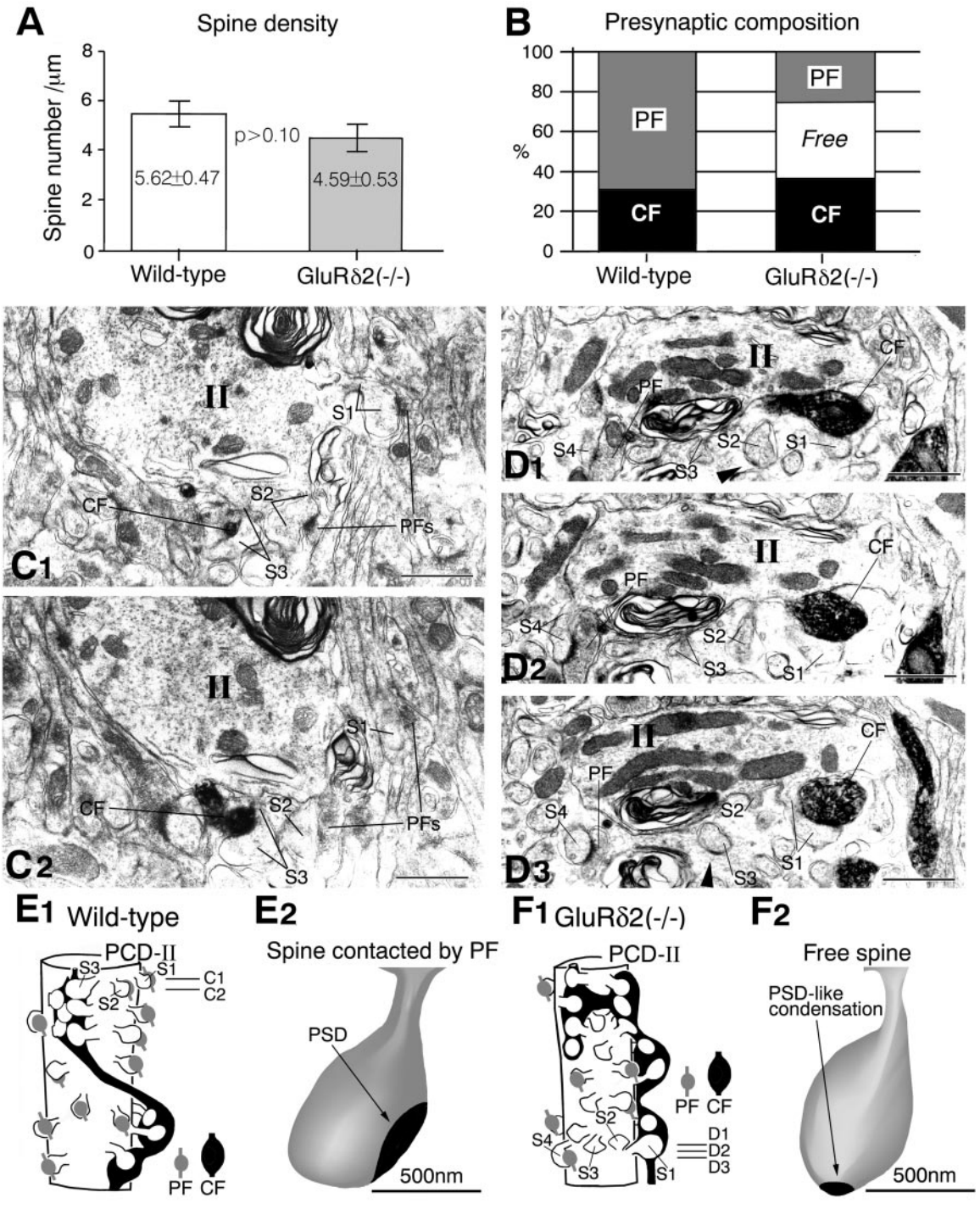

Figure 4. PCD-II (intermediate) domain. *A*, Spine density. *B*, Presynaptic composition on PC spines. *C1, C2*, Serial electron micrographs in the wild-type mouse. All spines protruding from the PCD-II domain (*II*), including those marked *S1–S3*, are contacted by either CFs or PFs. *D1–D3*, Serial electron micrographs in the knock-out mouse. Spines *S1* and *S4* are contacted by CF or PF, respectively, whereas spines *S2* and *S3* are free of innervation. A rudimentary postsynaptic density (PSD)-like condensation (*arrowheads*) is seen on free spines in the knock-out mouse. *Lines* emitting from marked spines point to either a spine head or spine neck connecting to dendrites. *E1, F1*, Reconstructed images of a part of the PCD-II domain. *E2, F2*, Three-dimensional reconstructed images for a single spine contacted by PF in the wild-type mouse and for a free spine in the knock-out mouse, respectively. PSD or PSD-like condensation is illustrated in *black*. Scale bars, 1 μm.

"pericellular nests" of CFs are displaced progressively toward "peridendritic" innervation onto stem dendrites; in the rat, the translocation is completed by postnatal day 15 (P15; Chédotal and Sotelo, 1992). At P7, when GluRδ2 targeting to PF synapses and dendritogenesis in PCs are both immature (Takayama et al., 1996), the contact rate between PF terminals and PC spines is similarly low in the wild-type and GluRδ2 knock-out mice (Kurihara et al., 1997). It is at the end of the second postnatal week that GluRδ2 targeting to PF synapses becomes efficient in wild-type rodents (Takayama et al., 1996; Zhao et al., 1998) and also when

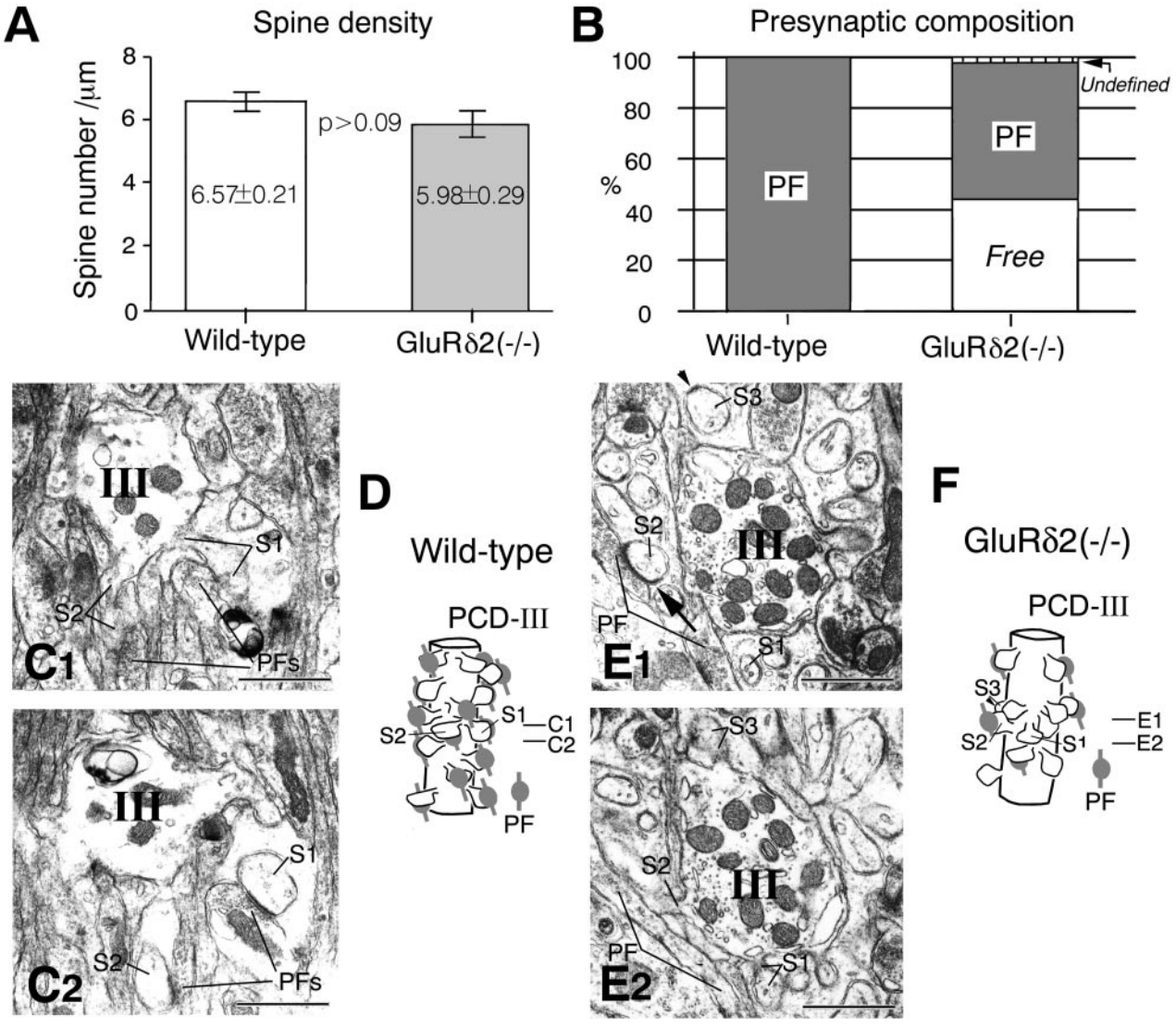

Figure 5. PCD-III (distal) domain. *A*, Spine density. *B*, Presynaptic composition on PC spines. *C1, C2*, Serial electron micrographs in the wild-type mouse. All spines, including *S1* and *S2*, are contacted by PFs. *E1, E2*, Serial electron micrographs in the knock-out mouse. Spine *S2* is contacted by PF, but spines *S1* and *S3* are free of innervation. The *arrow* in *E1* indicates elongated postsynaptic density that exceeds over the synaptic junction between the PF terminal and spine *S2*. *D, F*, Reconstructed images of a part of the PCD-III domain. Scale bars, 1 μm.

9the difference in the synaptic contact rate becomes evident between the two mouse strains (Kurihara et al., 1997). These results suggest that GluRδ2 is essential to prevent excessive distal translocation of CFs by consolidating late-differentiating distal dendrites for PF synapse formation. In this respect, GluRδ2 may play roles in shaping the territorized innervation by CFs and PFs, sharpening the border between the two territories (i.e., PCD-II domain) and ensuring full development of the PF territory. In the knock-out mouse, the PCD-I domain was significantly shortened despite weakened PF synaptogenesis. This implies that the full development of the CF territory may require the establishment of monoinnervation by CFs or reciprocal trophic interactions through competitive synaptogenesis by PFs and CFs.

Multiple CF innervation by excess wiring onto adjacent spiny branchlets

Surplus CFs are eliminated one by one, and a single winner finally establishes its innervation all over the proximal dendritic segment (Woodward et al., 1974; Mariani and Changeux, 1981a,b; Crépel, 1982). The elimination also proceeds actively around the end of the second postnatal week (Crépel et al., 1981; Chédotal and Sotelo, 1992). In the GluRδ2 knock-out mouse, the persistence of multiple CF innervation has been demonstrated electrophysiologically for nearly half of recorded PCs (Kashiwabuchi et al., 1995) or more (Hashimoto et al., 2001), although a much lower percentage (19~20%) is reported in hotfoot mutants (Lalouette et al., 2001). We first held that plexus-like CF innervation at proximal dendrites might be the morphological basis for multiple CF innervation in the GluRδ2 knock-out mouse. However, this was soon judged not to be the case. The dense plexus represents substantially, if not all, extensive collateral formation from a single parent CF. Unaltered spine density in the PCD-I domain further indicates that the collateral formation does not mean hyperinnervation to proximal dendrites. Rather, this may stand for hyperproduction of CF branches and tendrils, presumably to

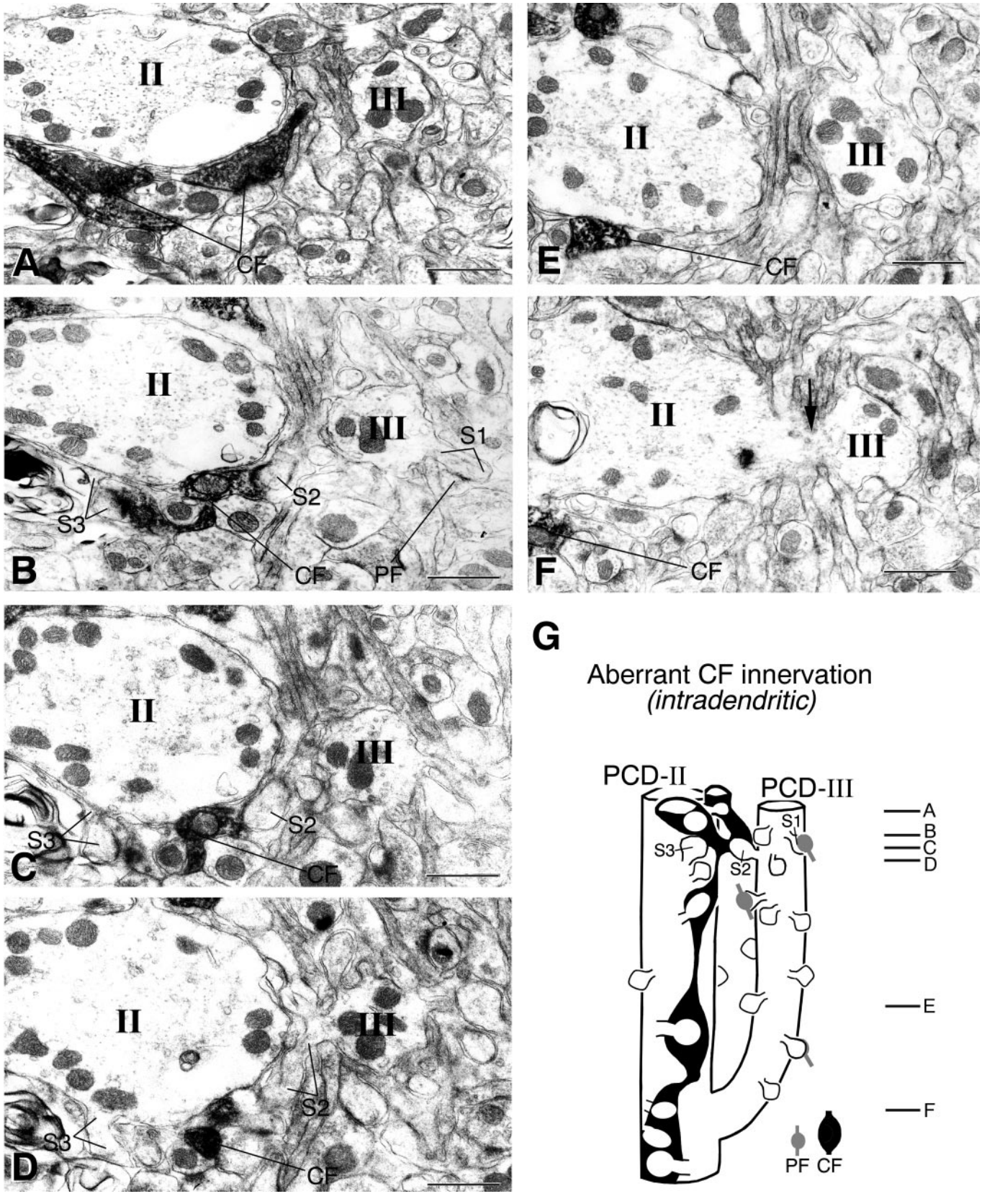

Figure 6. Serial electron micrographs showing aberrant CF innervation against adjacent spiny branchlets of the same PC in the GluRδ2 knock-out mouse. A labeled CF ascending the PCD-II dendrite (*II*) forms synaptic contact with spine *S2* (*B, C*). Spine *S2* protrudes from an adjacent spiny branchlet (*D, III*), which is branched from that PCD-II dendrite in a deeper region of the molecular layer (*F, arrow*). Spines *S1* and *S3* protrude from the PCD-III or PCD-II dendrite and are innervated by PF or labeled CF, respectively. *Lines* emitting from marked spines point to either a spine head or spine neck connecting to dendrites. *G*, Reconstructed image of the "intradendritic type" of aberrant CF innervation. Scale bars, 1 μm.

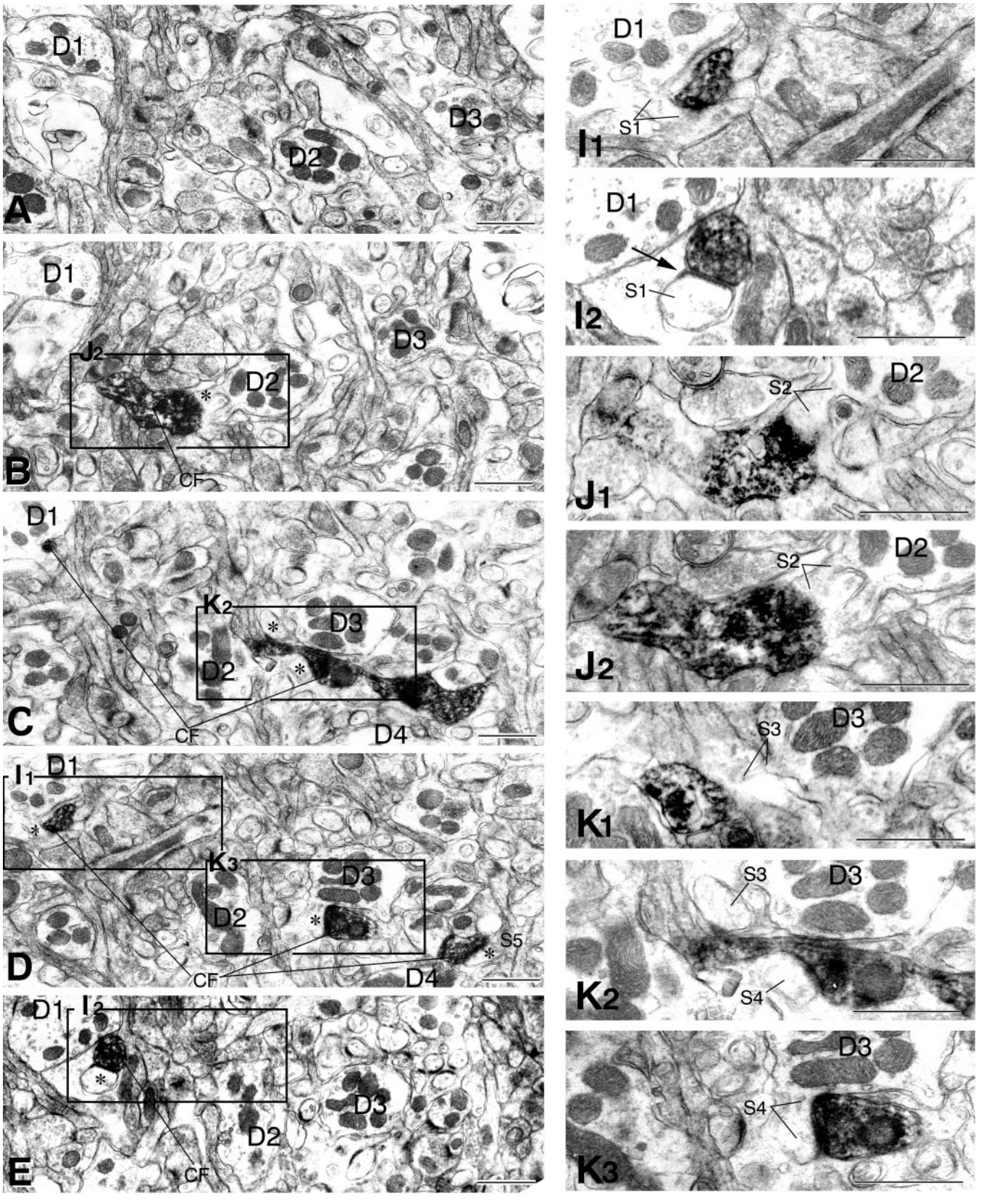

Figure 7. Serial electron micrographs showing aberrant CF jumping that causes multiple innervation in the GluRδ2 knock-out mouse. *A–H* are taken from levels indicated in reconstructed image *N*. To show synaptic contacts of the labeled CF with dendrites *D1–D4*, *boxed regions* in *A–H* are enlarged and provided with adjacent images as *I1, I2, J1, J2, K1–K3, L1–L3*, and *M1–M3*. The *arrow* in *I2* indicates elongated postsynaptic density exceeding over a synaptic junction between the CF terminal and spine *S1*. Note unlabeled CFs, *uCF1* (*L1–L3*) and *uCF2* (*M1–M3*), both of which form large terminal swellings with densely packed vesicles and ascend along the *D2* or *D3* dendrite, respectively. *uCF1* and *uCF2* form asymmetrical synapses with spine *S6* or spines *S7* and *S8*, respectively. Scale bars, 1 μm. (*Figure 7 continues.*)

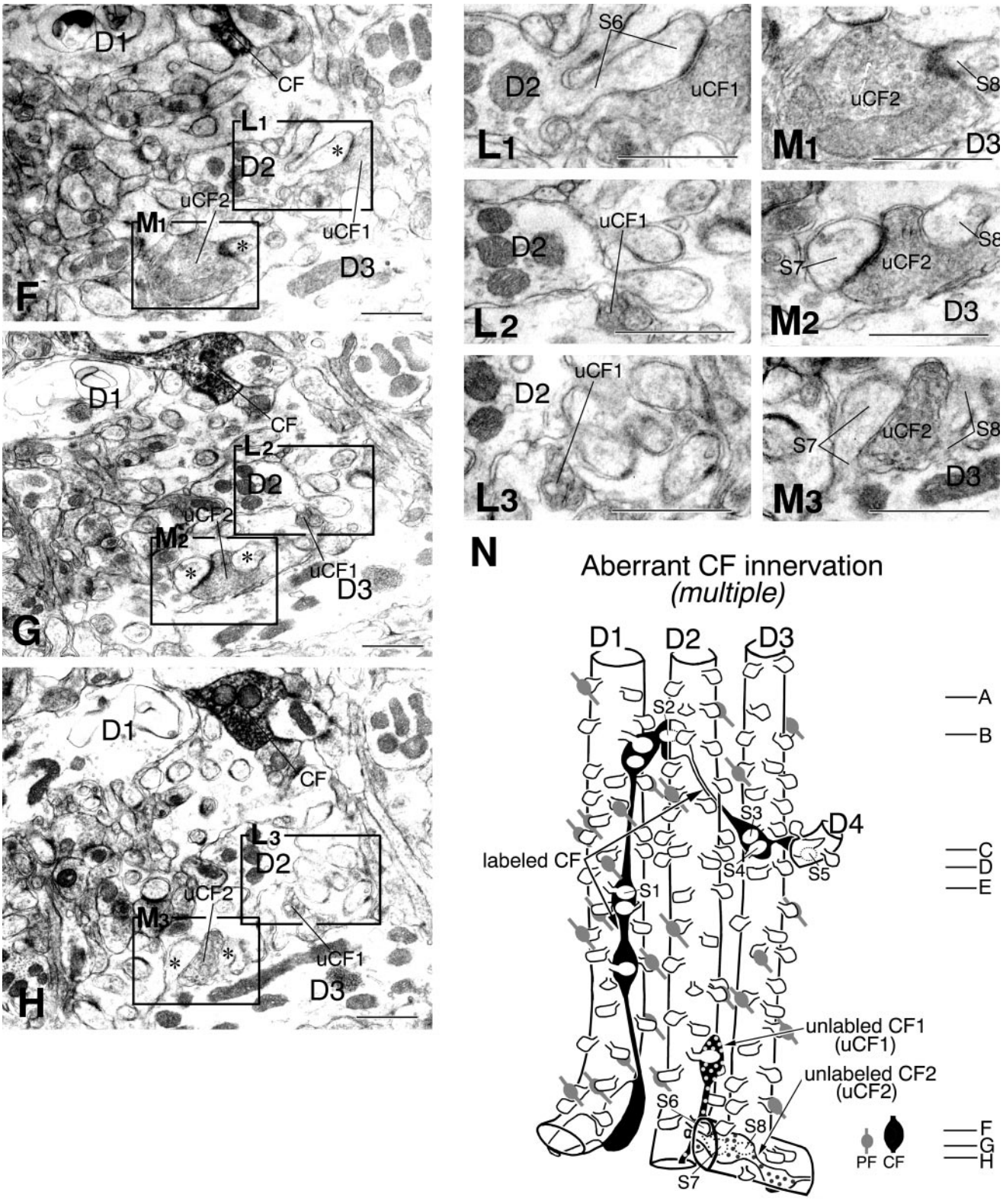

Figure 7 continued.

distribute them to innervate more distal dendrites, as a result of distal extension of the CF territory. How is multiple CF innervation formed in the GluRδ2 knock-out mouse?

In this regard, aberrant CF jumping to adjacent spiny branchlets should be noteworthy. In hypogranular cerebella of rats induced by methylazoxymethanol acetate administration, Zagrebelsky and Rossi (1999) have also documented the growth of CFs up to the pial surface and the occurrence of aberrant jumping from dendrites of one PC to those of a neighboring PC. We further addressed that aberrant jumping often caused dual

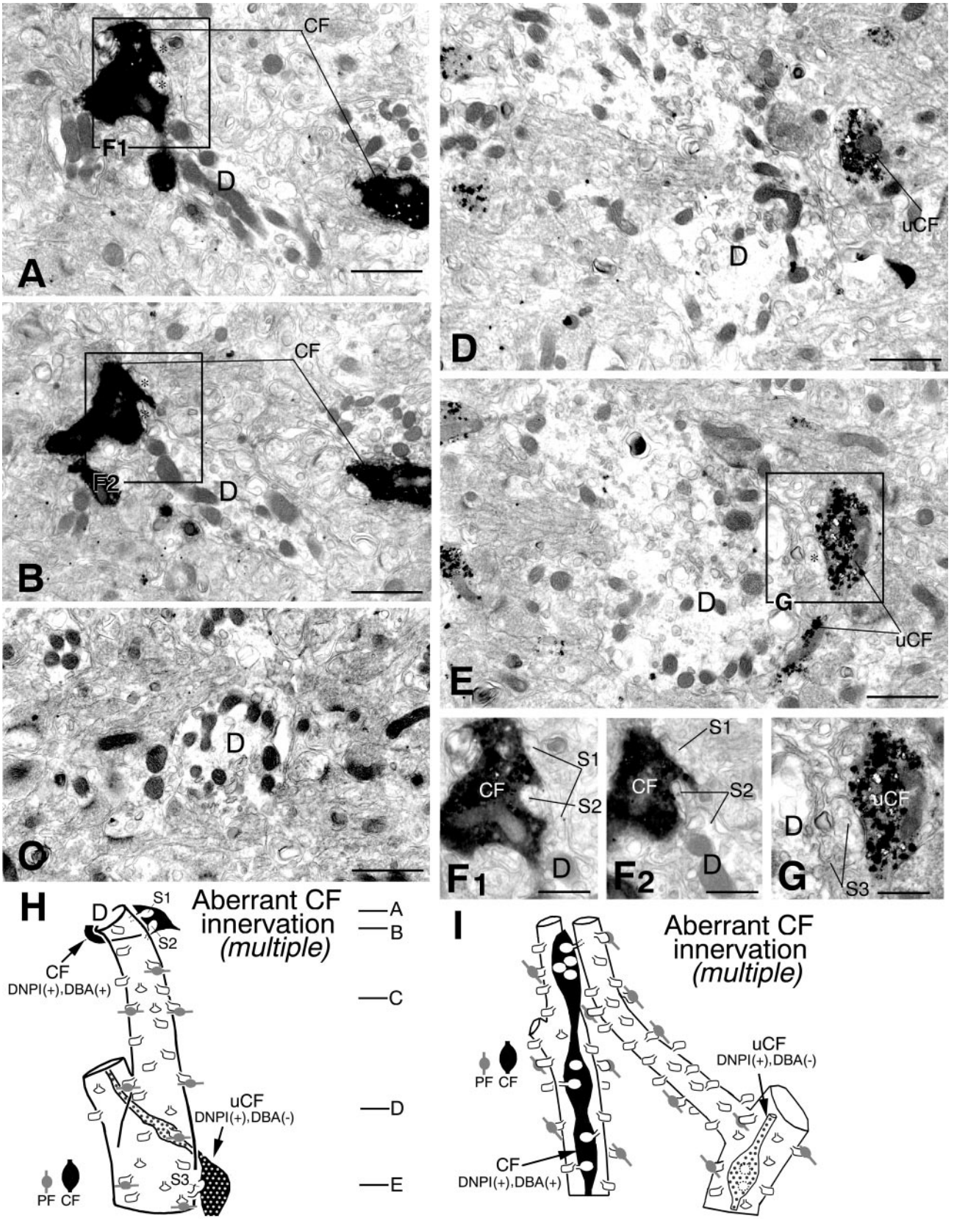

Figure 8. Combined anterograde labeling and DNPI immunolabeling demonstrating multiple CF innervation in the GluRδ2 knock-out mouse. *A–E* are taken from levels indicated in reconstructed image *H*. To show synaptic contacts of spines *S1–S3* with CFs, *boxed regions* in *A, B*, and *E* are enlarged as *F1, F2*, and *G*. Note that dendrites originating from the same PC (*D*) are innervated by anterogradely labeled (*CF* in *F1, F2*) and anterogradely unlabeled (*uCF* in *G*) CFs, both being heavily labeled by silver-intensified immunogold particles representing vesicular glutamate transporter DNPI. Another case of multiple innervation by anterogradely labeled and unlabeled CFs is shown as reconstructed image *I*. Scale bars: *A–E*, 1 μm; *F, G*, 0.5 μm.

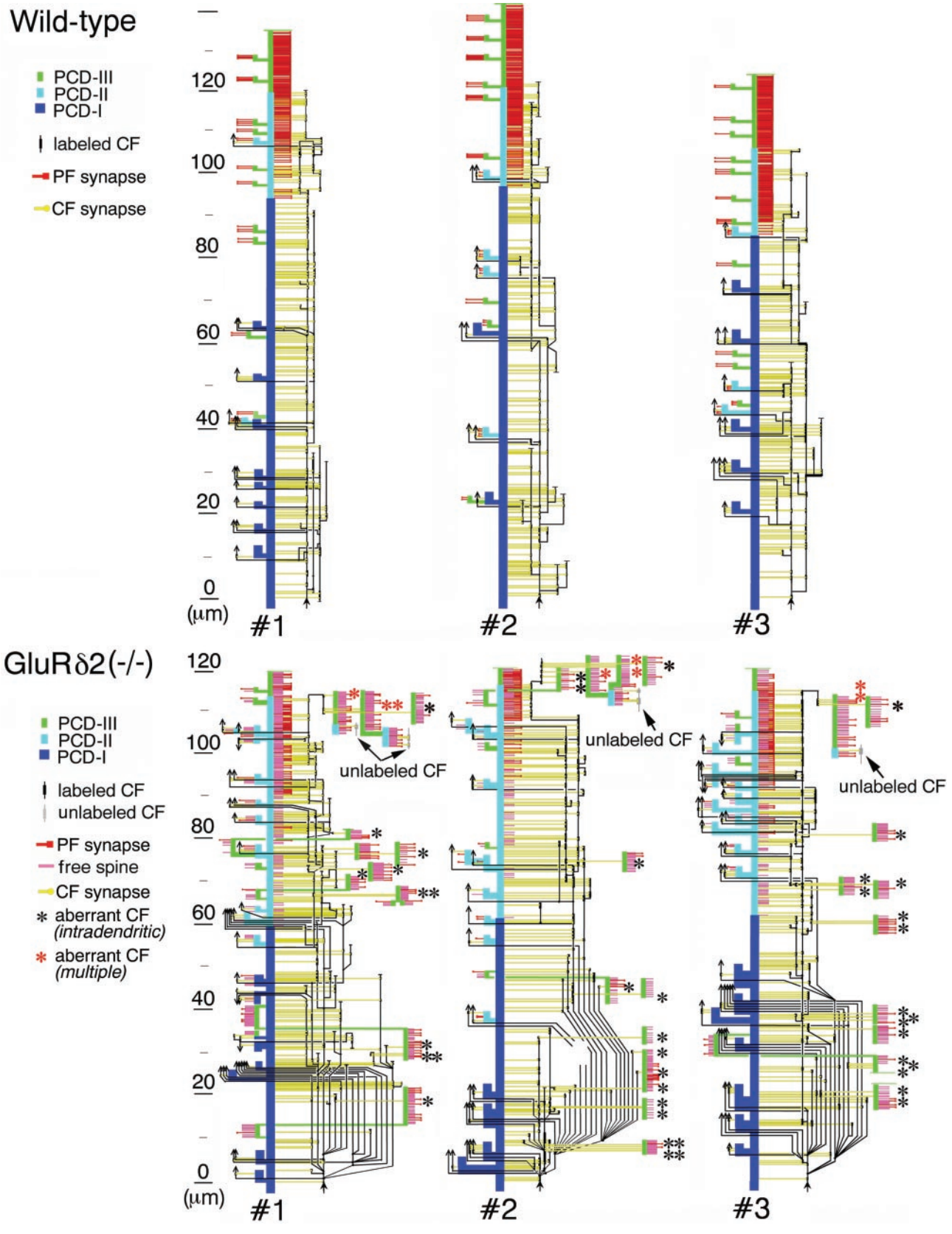

Figure 9. Schematic representation of CF and PF wiring onto PC dendrites. CF branches are shown as *black lines*. Aberrant CF innervation against adjacent PC dendrites is frequent and indicated by *asterisks*. In particular, aberrant innervation resulting in true dual innervation is indicated by *red asterisks*. PC spines contacted by CFs and PFs are represented as *yellow* and *red horizontal bars*, respectively, whereas free spines are represented as *pink horizontal bars*. The PCD-I, -II, and -III domains of PC dendrites are *dark blue*, *light blue*, and *green*, respectively. The vertical height of PC dendrites is shown to the *left*, starting from the initial CF branching point (*arrows*).

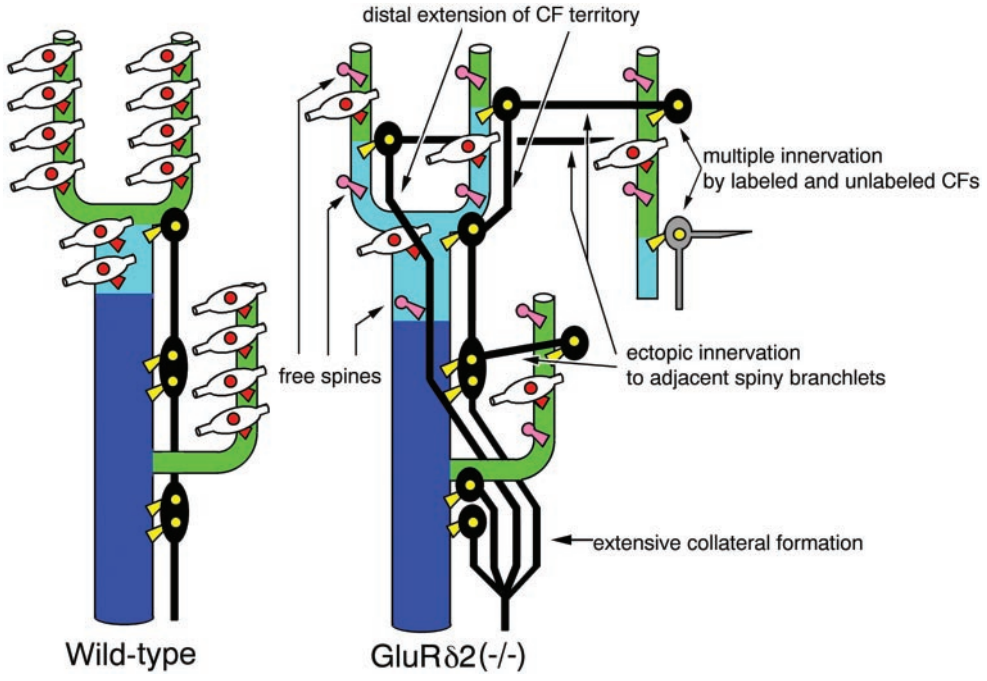

Figure 10. Summary of phenotypic differences in the GluRδ2 knock-out mouse. In the wild-type mouse, territories by CFs (*dark blue*) and PFs (*green*) are well segregated along the proximal-to-distal axis of PC dendrites, being connected by a short intermediate segment with mixed CF–PF innervation (*light blue*). In the knock-out mouse, CFs produce numerous collaterals, which extend distally to spiny branchlets. CFs often exceed the innervating dendrites and jump to form ectopic synapses on adjacent spiny branchlets. Such aberrant jumping sometimes causes multiple innervation of a given PC by anterogradely labeled and unlabeled CFs.

innervation of the same dendrite by anterogradely labeled and unlabeled CFs, i.e., multiple innervation by CFs with different neuronal origins. Despite that our analysis was limited to a particular track of CF arbors, such a true multiple type of CF innervation was observed in all three of the knock-out cases examined, indicating that it is a very common phenotype. In addition, aberrant CF jumping occurred after reaching the distal end point of innervation. On the basis of these findings, the form of multiple CF innervation in the GluRδ2 knock-out mouse can be depicted as follows. The main CF, the winner of the competition among multiple CFs, predominantly takes over the proximal dendritic segment. The main CF further sends its collaterals distally to innervate spiny branchlets having available postsynaptic substrates, i.e., free spines. The main CF often exceeds dendritic trees of the innervating PC and gives additional wiring to spiny branchlets of adjacent PCs. This additional wiring occurs mutually among neighboring PCs, leading to a high incidence of multiple CF innervation characteristic to this mutant.

This notion is consistent with our electrophysiological and Ca^{2+} imaging data (Hashimoto et al., 2001). In both GluRδ2 knock-out and wild-type mice, CF stimulation elicits typical EPSCs with a fast rise time and a large amplitude in a recorded PC. In addition to the main response, most knock-out PCs display additional steps of atypical CF EPSCs with a slow rise time and a small amplitude. Importantly, the activation of the main CF induces the spread of voltage-dependent Ca^{2+} signals all over the dendritic tree in both mice, whereas that of atypical CFs in the knock-out mouse elicits local Ca^{2+} signals confined to small distal regions of the dendritic tree. Atypical CFs may represent additional CFs coming from neighboring PCs to the recorded PC. Electrophysiological recording has also documented that some PCs in the GluRδ2 knock-out mouse exhibit multiple steps consisting of typical CF EPSCs only (Hashimoto et al., 2001). This suggests that additional CF wiring might also occur at proximal dendrites. Multiple CF innervation by overlapping innervation against the same dendrites (Sugihara et al., 2000) or by segregated coverage of dendritic arbors (Bravin et al., 1995) has been shown by CF labeling in hypogranular cerebella, where PF synapse formation is so severely lesioned as to affect the cerebellar histoarchitecture and differentiation of PC dendrites, especially the distal segment. In the present study, neither of these forms was substantiated, but additional CF wiring to more proximal dendrites might also exist in the GluRδ2 knock-out mouse.

Heterosynaptic competition between CFs and PFs

The present study eventually highlighted that GluRδ2 is a molecular substrate for heterosynaptic competition at PC dendrites, in which it stabilizes PF synapses and restricts CF innervation to the proximal dendritic segment. What then are the mechanisms that strengthen CF synapses and restrict PF innervation distally? When CFs are lesioned, the formation of new spines is induced from proximal dendrites, and PF innervation extends downward to proximal dendrites (Sotelo et al., 1975; Bradley and Berry, 1976; Sotelo and Arsenio-Nunes, 1976; Sotelo, 1978; Desclin and Colin, 1980; Angaut et al., 1982; Baetens et al., 1982; Rossi et al., 1991). Similar phenomena are observed when electrical activity is depressed by tetrodotoxin administration to the adult cerebellum (Bravin et al., 1999). Such a hyperspiny transformation of proximal dendrites also occurs in mutant mice with spontaneous gene mutations of the voltage-dependent Ca^{2+} channel α1A subunit, such as the rolling mouse Nagoya, tottering, and leaner (Rhyu et al., 1999), although how CFs innervate PC dendrites remains elusive in these mutants. These results suggest that CF activities that lead to strong excitation and Ca^{2+} entry to PC dendrites are crucial to inhibit the expansion of the PF territory. Thus, the two inputs are highly plastic and competitive and use different cellular and molecular mechanisms to strengthen their own territory at the expense of the other. Armed with both mechanisms, heterosynaptic competition between CFs and PFs is properly fueled, and synaptic wiring is normally structured on PC dendrites. It has been shown that tetrodotoxin treatment disrupts selective localization of GluRδ2 at PF synapses and induces its redistribution to other synapses in adult PCs (Morando et al., 2001), suggesting activity-dependent control of GluRδ2-dependent mechanisms.

In conclusion, GluRδ2 is essential to restrict CF innervation to the proximal dendritic segment of the target PC. Without GluRδ2, the CF territory expands distally along and beyond dendritic trees of the target PCs, causing persistent multiple CF innervation.

REFERENCES

Aiba A, Kano M, Chen C, Stanton ME, Fox GD, Herrup K, Zwingman TA, Tonegawa S (1994) Deficient cerebellar long-term depression and impaired motor learning in mGluR1 mutant mice. Cell 79:377–388.

Altman J (1972) Postnatal development of the cerebellar cortex in the rat. II. Phases in the maturation of Purkinje cells and of the molecular layer. J Comp Neurol 145:399–463.

Angaut P, Alvarado-Mallart RM, Sotelo C (1982) Ultrastructural evidence for compensatory sprouting of climbing and mossy afferents to the cerebellar hemisphere after ipsilateral pedunculotomy in the newborn rat. J Comp Neurol 205:101–111.

Araki K, Meguro H, Kushiya E, Takayama C, Inoue Y, Mishina M (1993) Selective expression of the glutamate receptor channel δ2 subunit in cerebellar Purkinje cells. Biochem Biophys Res Commun 197:1267–1276.

Baetens D, Garcia-Segura LM, Perrelet A (1982) Effects of climbing fiber destruction on large dendrite spines of Purkinje cells. Exp Brain Res 48:256–262.

Bradley P, Berry M (1976) Quantitative effects of climbing fibre deafferentation on the adult Purkinje cell dendritic tree. Brain Res 112:133–140.

Bravin M, Rossi F, Strata P (1995) Different climbing fibres innervate separate dendritic regions of the same Purkinje cell in hypogranular cerebellum. J Comp Neurol 357:395–407.

Bravin M, Morando L, Vercelli A, Rossi F, Strata P (1999) Control of spine formation by electrical activity in the adult rat cerebellum. Proc Natl Acad Sci USA 96:1704–1709.

Chédotal A, Sotelo A (1992) Early development of the olivocerebellar projections in the fetal rat using CGRP-immunocytochemistry. Eur J Neurosci 4:1159–1179.

Chen S, Hillman DE (1982) Plasticity of the parallel fiber-Purkinje cell synapse by spine takeover and new synapse formation in the adult rat. Brain Res 240:205–220.

Conquet F, Bashir ZI, Davies CH, Daniel H, Ferraguti F, Bordi F, Franz-Bacon K, Reggiani A, Matarese V, Conde F, Collingridge GL, Crépel F (1994) Motor deficit and impairment of synaptic plasticity in mice lacking mGluR1. Nature 372:237–243.

Crépel F (1982) Regression of functional synapses in the immature mammalian cerebellum. Trends Neurosci 5:266–269.

Crépel F, Delhaye-Bouchaud JL, Dupont JL (1981) Fate of the multiple innervation of cerebellar Purkinje cells by climbing fibers in immature control, X-irradiated and a hypothyroid rats. Brain Res Dev Brain Res 1:59–71.

Desclin JC, Colin F (1980) The olivocerebellar system, II. Some ultrastructural correlates of inferior olive destruction in the rat. Brain Res 187:29–46.

Fremeau Jr RT, Troyer MD, Pahner I, Nygaard GO, Tran CH, Reimer RJ, Bellocchio EE, Fortin D, Storm-Mathisen J, Edwards RH (2001) The expression of vesicular glutamate transporters defines two classes of excitatory synapse. Neuron 31:247–260.

Funabiki K, Mishina M, Hirano T (1995) Retarded vestibular compensation in the mutant mice deficient of δ2 glutamate receptor subunit. NeuroReport 7:189–192.

Guastavino JM, Sotelo C, Damez-Kinselle I (1990) Hot-foot murine mutation: behavioral effects and neuroanatomical alterations. Brain Res 523:199–210.

Hashimoto K, Ichikawa R, Takechi H, Inoue Y, Aiba A, Sakimura K, Mishina M, Hashikawa T, Konnerth A, Watanabe M, Kano M (2001) Roles of GluRδ2 and mGluR1 in climbing fiber synapse elimination during postnatal cerebellar development. J Neurosci 21:9701–9712.

Ichise T, Kano M, Hashimoto K, Yanagihara D, Nakao K, Shigemoto R, Katsuki M, Aiba A (2000) mGluR1 in cerebellar Purkinje cells essential for long-term depression synapse elimination and motor coordination. Science 288:1832–1835.

Ito M (1989) Long-term depression. Annu Rev Neurosci 12:85–102.

Kano M, Hashimoto K, Chen C, Abeliovich A, Aiba A, Kurihara H, Watanabe M, Inoue Y, Tonegawa S (1995) Impaired synapse elimination during cerebellar development in PKCγ mutant mice. Cell 83:1223–1231.

Kano M, Hashimoto K, Kurihara H, Watanabe M, Inoue Y, Aiba A, Tonegawa S (1997) Persistent multiple climbing fiber innervation of cerebellar Purkinje cells in mice lacking mGluR1. Neuron 18:71–79.

Kano M, Hashimoto K, Watanabe M, Kurihara H, Offermanns S, Jiang H, Wu Y, Jun K, Shin HS, Inoue Y, Simon MI, Wu D (1998) Phospholipase Cβ4 is specifically involved in climbing fiber synapse elimination in the developing cerebellum. Proc Natl Acad Sci USA 95:15724–15729.

Kashiwabuchi N, Ikeda K, Araki K, Hirano T, Shibuki K, Takayama C, Inoue Y, Kutsuwada T, Yagi T, Kang Y, Aizawa S, Mishina M (1995) Impairment of motor coordination Purkinje cell synapse formation and cerebellar long-term depression in GluRδ2 mutant mice. Cell 81:245–252.

Kishimoto Y, Kawahara S, Suzuki M, Mori H, Mishina M, Kirino Y (2001) Classical eyeblink conditioning in glutamate receptor subunit δ2 mutant mice is impaired in the delay paradigm but not in the trace paradigm. Eur J Neurosci 13:1249–1253.

Kohda K, Wan Y, Yuzaki M (2000) Mutation of a glutamate receptor motif reveals its role in gating and δ2 receptor channel properties. Nat Neurosci 3:315–322.

Kurihara H, Hashimoto K, Kano M, Takayama C, Sakimura K, Mishina M, Inoue Y, Watanabe M (1997) Impaired parallel fiber-Purkinje cell synapse stabilization during cerebellar development of mutant mice lacking the glutamate receptor δ2 subunit. J Neurosci 17:9613–9623.

Lalouette A, Lohof A, Sotelo C, Guenet J, Mariani J (2001) Neurobiological effects of a mull mutation depend on genetic context: comparison between two hotfoot alleles of the delta-2 ionotropic glutamate receptor. Neuroscience 105:443–455.

Landsend AS, Amiry-Moghaddam M, Matsubara A, Bergersen L, Usami S, Wenthold RJ, Ottersen OP (1997) Differential localization of delta glutamate receptors in the rat cerebellum: coexpression with AMPA receptors in parallel fiber-spine synapses and absence from climbing fiber-spine synapses. J Neurosci 17:834–842.

Larramendi LMH, Victor T (1967) Synapses on the Purkinje cell spines in the mouse an electronmicroscopic study. Brain Res 5:15–30.

Linden DJ, Connor JA (1995) Long-term synaptic depression. Annu Rev Neurosci 18:319–357.

Lomeli H, Sprengel R, Laurie DJ, Kohr G, Herb A, Seeburg PH, Wisden W (1993) The rat delta-1 and delta-2 subunits extend the excitatory amino acid receptor family. FEBS Lett 315:318–322.

Mariani J (1982) Extent of multiple innervation of Purkinje cells by climbing fibers in the olivocerebellar system of weaver reeler and staggerer mutant mice. J Neurobiol 13:119–126.

Mariani J, Changeux JP (1981a) Ontogenesis of olivocerebellar relationships. I. Spontaneous activity of inferior olivary neurons and climbing fiber mediated activity of cerebellar Purkinje cells in developing rats. J Neurosci 1:696–702.

Mariani J, Changeux JP (1981b) Ontogenesis of olivocerebellar relationships. II. Spontaneous activity of inferior olivary neurons and climbing fiber mediated activity of cerebellar Purkinje cells in developing rats. J Neurosci 1:703–709.

Morando L, Cesa R, Rasetti R, Harvey R, Strata P (2001) Role of glutamate δ-2 receptors in activity-dependent competition between heterologous afferent fibers. Proc Natl Acad Sci USA 98:9954–9959.

Nakagawa S, Watanabe M, Isobe T, Kondo H, Inoue Y (1998) Cytological compartmentalization in the staggerer cerebellum, as revealed by calbindin immunohistochemistry for Purkinje cells. J Comp Neurol 395:112–120.

Napper RM, Harvey RJ (1988) Number of parallel fiber synapses on an individual Purkinje cell in the cerebellum of the rat. J Comp Neurol 274:168–177.

Offermanns S, Hashimoto K, Watanabe M, Sun W, Kurihara H, Thompson RF, Inoue Y, Kano M, Simon MI (1997) Impaired motor coordination and persistent multiple climbing fiber innervation of cerebellar Purkinje cells in mice lacking Gαq. Proc Natl Acad Sci USA 94:14089–14094.

Palay S, Chan-Palay V (1974) Cerebellar cortex: cytology and organization. New York: Springer.

Rhyu IJ, Oda S, Uhm CS, Kim H, Suh YS, Abbott LC (1999) Morphologic investigation of rolling mouse Nagoya (tg(rol)/tg(rol)) cerebellar Purkinje cells: an ataxic mutant revisited. Neurosci Lett 266:49–52.

Rossi F, van der Want JJ, Wiklund L, Strata P (1991) Reinnervation of cerebellar Purkinje cells by climbing fibres surviving a subtotal lesion of the inferior olive in the adult rat, II. Synaptic organization on reinnervated Purkinje cells. J Comp Neurol 308:536–554.

Rossi F, Jankovski A, Sotelo C (1995) Target neuron controls the integrity of afferent axon phenotype: a study on the Purkinje cell-climbing fiber system in cerebellar mutant mice. J Neurosci 15:2040–2056.

Sotelo C (1978) Purkinje cell ontogeny: formation and maintenance of spines. Prog Brain Res 48:149–170.

Sotelo C, Arsenio-Nunes ML (1976) Development of Purkinje cells in absence of climbing fibers. Brain Res 111:289–295.

Sotelo C, Hillman DE, Zamora AJ, Llinas R (1975) Climbing fiber deafferentation: its action on Purkinje cell dendritic spines. Brain Res 98:574–581.

Strata P, Rossi F (1998) Plasticity of the olivocerebellar pathway. Trends Neurosci 21:407–413.

Sugihara I, Bailly Y, Mariani J (2000) Olivocerebellar climbing fibers in

the granuloprival cerebellum: morphological study of individual axonal projections in the X-irradiated rat. J Neurosci 20:3745–3760.
Takács J, Hámori J (1994) Developmental dynamics of Purkinje cells and dendritic spines in rat cerebellar cortex. J Neurosci Res 38:515–530.
Takayama C, Nakagawa S, Watanabe M, Mishina M, Inoue Y (1996) Developmental changes in expression and distribution of the glutamate receptor channel δ2 subunit according to the Purkinje cell maturation. Brain Res Dev Brain Res 92:147–155.
Takeuchi T, Kiyama Y, Nakamura K, Tsujita M, Matsuda I, Mori H, Munemoto Y, Kuriyama H, Natsume R, Sakimura K, Mishina M (2001) Roles of the glutamate receptor ε2 and δ2 subunits in the potentiation and prepulse inhibition of the acoustic startle reflex. Eur J Neurosci 14:153–160.
Wollmuth LP, Kuner T, Jatzke C, Seeburg PH, Heintz N, Zuo J (2000) The Lurcher mutation identifies δ2 as an AMPA/kainate receptor-like channel that is potentiated by Ca^{2+}. J Neurosci 20:5973–5980.
Woodward DJ, Hoffer BJ, Siggins GR, Bloom FE (1971) The ontogenetic development of synaptic junctions, synaptic activation and responsiveness to neurotransmitter substances in rat cerebellar Purkinje cells. Brain Res 34:73–97.
Woodward DJ, Hoffer BJ, Altman J (1974) Physiological and pharmacological properties of Purkinje cells in rat cerebellum degranulated by postnatal x-irradiation. J Neurobiol 5:283–304.
Xu-Friedman MA, Harris KM, Regehr WG (2001) Three-dimensional comparison of ultrastructural characteristics at depressing and facilitating synapses onto cerebellar Purkinje cells. J Neurosci 21:6666–6672.
Zagrebelsky M, Rossi F (1999) Postnatal development and adult organization of the olivocerebellar projection map in the hypogranular cerebellum of the rat. J Comp Neurol 407:527–542.
Zhao JM, Wenthold RJ, Petralia RS (1998) Glutamate receptor targeting to synaptic populations on Purkinje cells is developmentally regulated. J Neurosci 18:5517–5528.
Zuo J, De Jager PL, Takahashi KA, Jiang W, Linden DJ, Heintz N (1997) Neurodegeneration in Lurcher mice caused by mutation in δ2 glutamate receptor gene. Nature 388:769–773.